Data Association for Moving Multitarget Sensing in Distributed OTFS Radars

Buyi Li, *Graduate Student Member, IEEE*, Dongxuan He, *Member, IEEE*, and Qin Tao, *Member, IEEE*

***Abstract*—Aerial drones in wireless communication systems offer rapid deployment, flexible reconfiguration, and superior communication channels, thanks to their short-range line-of-sight links, making them more efficient and cost-effective than terrestrial or high-altitude platform networks. As a promising technique, integrated sensing and communication (ISAC) enhances aerial drones networks by integrating sensing and communication functionalities. This concurrent design improves spectrum efficiency and reduces hardware costs. To ensure reliable communication for their high mobility, a novel modulation technique, the orthogonal time-frequency space (OTFS) waveform, has been proposed, which leverages the delay-Doppler domain for efficient information transmission. In this article, we investigate ISAC-based multitarget sensing with distributed OTFS radars to deliver reliable performance for aerial drones networks. To achieve that, we propose to leverage the delay and Doppler information featured by OTFS signals to determine the range and radial velocity, accomplishing successful sensing tasks. Moreover, to address the challenge of unassociated measurements and targets, we propose a novel optimization framework to concurrently perform data association and target sensing tasks. This framework is developed by formulating a mixed-integer optimization problem, which is then solved with polynomial complexity through convex approximation. Additionally, we propose an iterative maximum likelihood estimator (MLE) to further enhance sensing performance by accounting for target-measurement errors. Extensive simulation results verify the superiority of our proposed work to state-of-the-art methods.**

***Index Terms*—Aerial drone, data association, integrated sensing and communication (ISAC), multitarget sensing, orthogonal time-frequency space (OTFS).**

I. Introduction

With their remarkable mobility and affordability, aerial drones, also known as drones or remotely piloted aircraft, have found widespread applications across various sectors over the past few decades [1], [2]. aerial drones, originally developed for military use to reduce pilot risks, have become more accessible due to advancements in technology. Small aerial drones are now widely used in civilian applications, such as weather monitoring, traffic control, and search and rescue. Aerial drones are classified into fixed-wing and rotary-wing types [3]. Fixed-wing aerial drones are fast and carry heavier payloads but need continuous forward motion. Rotary-wing aerial drones, like quadcopters, can hover and move in any direction but have limited payload and range. The choice depends on the specific application.

Among the various applications enabled by aerial drones, both communication and sensing functionalities are essential for ensuring the effectiveness of their operations [4]. Specifically, aerial drones demand advanced communication systems that provide high bandwidth, low latency, and constant connectivity to facilitate seamless data exchange within the aerial drones network. Meanwhile, accurate target states obtained by the sensing function, e.g., location and velocity, enable precise real-world representation, which can improve situational awareness, detect obstacles, and monitor environmental conditions more effectively. Although sensing and communication share similar radio frequency (RF) components and signal-processing techniques, they were historically implemented using separate systems [5], [6]. While separate designs minimize mutual interference, they waste spectral resources and increase implementation costs [7], [8]. Given scarce frequency bands and financial constraints, integrating the two functions offers a promising alternative, inspiring the development of integrated sensing and communication (ISAC) [9], [10]. Its core insight lies in enabling sensing and communication to share a unified hardware architecture, spectral resources, and signal processing framework, enhancing efficiency and system performance [11].

Building upon ISAC principles, distributed communication radars have gained growing attention for facilitating sensing tasks by extracting various measurements from transmitted signals, including time delay (TD), angle of arrival (AOA), direction of arrival (DOA), and Doppler shift. These measurements are then processed to estimate target parameters, e.g., position and velocity. For instance, with a bistatic transmitter-receiver pair, TD can be converted into range information for localization, while Doppler shift is a key factor for radial velocity estimation. Additionally, combining TD and Doppler shifts can determine the locations of moving targets. Recognizing these benefits, substantial efforts have been

Received 19 February 2025; revised 19 April 2025 and 19 May 2025; accepted 2 June 2025. Date of publication 11 June 2025; date of current version 5 February 2026. This work was supported in part by the National Natural Science Foundation of China under Grant 62471208; in part by the Guangdong Provincial Natural Science Foundation under Grant 2024A151510098; in part by the Shenzhen Science and Technology Program under Grant JCYJ20220530114412029; and in part by the National Key Research and Development Program of China under Grant 2024YFE0200404. *(Corresponding author: Dongxuan He.)*

Buyi Li is with the School of System Design and Intelligent Manufacturing, Southern University of Science and Technology, Shenzhen 518055, China (e-mail: liby2022@mail.sustech.edu.cn).

Dongxuan He is with the School of Information and Electronics, Beijing Institute of Technology, Beijing 100081, China (e-mail: dongxuan_he@bit.edu.cn).

Qin Tao is with the School of Information Science and Technology, Hangzhou Normal University, Hangzhou 311121, China (e-mail: taoqin@hznu.edu.cn).

Digital Object Identifier 10.1109/JIOT.2025.3578819

devoted to advancing the communication radars for ISAC, with orthogonal frequency division multiplexing (OFDM) commonly employed for its potential in both communication and sensing applications. Specifically, OFDM offers significant advantages in communications, including low-complexity data detection, robustness to frequency selectivity, and flat fading across subcarriers. Furthermore, OFDM signals include essential information for target sensing, e.g., TD, angle, and Doppler, which can be extracted from its channel estimation process.

Given its promise, OFDM channel estimation for sensing has been extensively investigated, particularly for TD and angle information. To name a few, the authors in [12] proposed a maximum likelihood estimator (MLE) for TD estimation, exploiting the redundancy of the cyclic prefix and the pilot symbols on the carriers. In [13], the authors designed a tailored training symbol to extract TD information in the additive white Gaussian noise (AWGN) channel. Moreover, a recent study [14] focused on angle information estimation, designing two subspace-based methods: 1) multiple-signal-classification (MUSIC) and 2) estimation-of-signal-parameters-via-rotational-invariance-techniques (ESPRIT) [14]. Despite progress in DT and angle estimation, estimating Doppler shifts in OFDM-based ISAC radars remains challenging. This is because Doppler shifts disrupt the orthogonality of OFDM subcarriers, introducing intercarrier interference (ICI) [15] and making accurate estimation difficult. To address this problem, a recent solution in [16] proposed an element-wise division-based method and leverages discrete Fourier transform (DFT) for independent range and Doppler estimation. To further enhance performance, [17] proposed a matrix algebra-based method to estimate range and Doppler jointly. However, these methods require a large number of OFDM symbols for high-frequency resolution and rely on computationally intensive filters to ensure performance, limiting their applicability. Consequently, OFDM-based radars are not well-suited for Doppler shift estimation, leading most OFDM-based sensing methods to focus on static target localization that utilizes solely TD or angle information.

Motivated by the above, orthogonal time-frequency space (OTFS) has been proposed as a promising alternative for sensing with ISAC radars [18]. OTFS modulates data symbols in the delay-Doppler (DD) domain rather than the conventional time-frequency (TF) domain in OFDM, offering stronger delay and Doppler resilience. By operating in the DD domain, OTFS achieves full TF diversity gain, mitigating fading over double-dispersive channels and ensuring reliable communication in dynamic and complex environments [19]. Furthermore, OTFS outperforms OFDM in sensing by transforming a time-varying channel into a 2-D quasi-time-invariant channel in the DD domain. This enables reliable estimation of delay and Doppler shifts, with various methods proposed to accomplish tasks, including pilot embedding [20], sparse Bayesian learning (SBL) [21], and the 3-D-structured orthogonal matching pursuit algorithm [22]. However, most existing works on OTFS-ISAC applications focus on sensing-assisted communication [23]. However, the potential of OTFS-assisted ISAC remains underexplored. OTFS signals in the DD domain can reveal the underlying wireless propagation environment. Specifically, DD domain characteristics, such as delay and Doppler, can be directly mapped to physical environmental information, such as range and relative speed. Therefore, OTFS communication presents a promising opportunity for environment sensing by leveraging DD domain channel estimation. Research on OTFS-assisted sensing remains limited, such as [24], [25] and [26].

Li and Yuan [24] studied an OTFS-based sensing problem with a single moving target and proposed a two-step strategy for task accomplishment. With a similar purpose, [25] formulated the OTFS sensing problem as a nonlinear weighted least squares (WLS) problem and solved it through Newton's method. Additionally, Wu et al. [26] designed a unified OTFS waveform to realize concurrent sensing and communication.

To further explore the potential of OTFS in sensing respects, we consider a general scenario with multiple moving targets and distributed OTFS radars. Different from the extensively studied single-target sensing problem, multitarget sensing typically requires a detection step. This is because receivers are unaware of the associations between extracted measurements and individual targets. These simultaneous reflections from multiple targets pose a substantial challenge to the sensing task. However, this target-measurement association step is not been well studied in the most existing works on sensing. They take full advantage of the received signal information and always attempt to directly localize multiple targets by jointly processing the unthresholded signal echoes and obtaining the MLE [27]. Hence, such algorithms, referred to as the direct sensing approaches, are robust, especially in low signal-to-noise ratio (SNR). In many practical scenarios, this kind of data association problem should be considered.

There are still quite a few studies in the literature for sensing consider this measurement-to-target association problem (MTAP), such as [28], [29], and [30]. These approaches are often referred to as the two-step localization approaches. Reference [28] proposes a basic iteration algorithm for MTAP, but it requires the prior target positions, which can restrict the application of this algorithm in many practical problems. The brute-force-based algorithms in [29] are inefficient to employ for each possible hypothesis due to their exponential complexity. An efficient method has been proposed in [30] by approximating MTAP to a convex problem, but it only considers the range measurements for static target localization.

To address the aforementioned challenges, this article develops a novel approach for multiple moving-target sensing, by leveraging the property of OTFS in high-speed mobile communication. Compared to traditional OFDM-based ISAC systems that require additional high-complexity operations to obtain Doppler information for the sensing purpose, e.g. [17], the OTFS-based system can directly provide Doppler information from DD domain, which is also utilized for OTFS communications. To elaborate, the transmitted OTFS signals are reflected by the moving multitarget, and received by receivers. We obtain the delay and Doppler information from OTFS channel estimation, which is utilized to estimate the target position and velocity. In particular, multitarget sensing requires

TABLE I
NOTATIONS AND SYMBOLS

Symbol	Description
d	Dimension of sensing
$\mathbb{R}^d$	d-dimensional space of real numbers
N_t	Number of transmitters
N_r	Number of receivers
$\mathbf{q}_i$	Position of transmitter i, $i = 1, 2, \ldots, N_t$
$\mathbf{p}_j$	Position of receiver j, $j = 1, 2, \ldots, N_r$
$\mathbf{s}_k$	Position of target k, $k = 1, 2, \ldots, K$
$\dot{\mathbf{s}}_k$	Velocity of target k, $k = 1, 2, \ldots, K$
B	Bandwidth
T_f	Time duration of a single OTFS frame
Δf	Subcarrier space
T	Symbol duration
X_{DD}	Transmitted symbol in DD domain
X_{TF}	Transmitted symbol in TF domain
$s(t)$	Radar transmitted waveform
Y_{DD}	Received symbol in DD domain
Y_{TF}	Received symbol in TF domain
$r(t)$	Radar received waveform
τ	Time delay of arrival
ν	Doppler-shift
$h(\tau, \nu)$	Complex baseband channel impulse response
$\omega(t)$	Additive white Gaussian noise process
c	Speed of signal propagation
f_c	Carrier frequency
r_{ij}^k	Bistatic range (BR) of the signal from transmitter i to received j, reflected by target k
$\dot{r}_{ij}^k$	Range rate (RR) of the signal from transmitter i to received j, reflected by target k
$\mathbf{G}_j$	Permutation matrix for observed measurements at receiver j
$\boldsymbol{\theta}$	Vector contains all target states, $\mathbf{s}_1, \mathbf{s}_2, \ldots, \mathbf{s}_K, \dot{\mathbf{s}}_1, \dot{\mathbf{s}}_2, \ldots, \dot{\mathbf{s}}_K$
$\mathbf{J}(\boldsymbol{\theta}^o)$	Fisher information matrix, eq(42)
L	Number of Monte Carlo runs
$(\cdot)^o$	True value of the variable $(\cdot)$

detection steps, since the receivers lack awareness of associations between the extracted measurements and individual targets. Most existing multitarget sensing methods are two-step methods, which require the prior target states, e.g. [28]. In contrast, our proposed method can concurrently perform data association and jointly estimate the target position and velocity. Unlike traditional two-step sensing methods that rely on prior target states, the proposed method performs data association and target state estimation jointly. To realize it, we formulate a mixed-integer optimization problem, which can be efficiently solved with a polynomial complexity by using first-order Taylor approximation and relaxed integer conditions to approximate. Because the constraints are relaxed and noise is not considered, the solution to the relaxed problem lacks sufficient accuracy. Using a grid-searching method to obtain MLE directly is prohibitive due to the high dimension of the unknown parameter space. However, relying on the preliminary solution can yield satisfactory accuracy for iteratively implementing MLE to improve precision. In particular, we adopt the Gauss-Newton MLE to obtain an accurate solution using the permuted measurements and preliminary solution.

The contributions of this work are summarized as follows.

1) We investigate multiple moving-target sensing problem and propose a novel framework based on distributed OTFS radars. By leveraging the delay and Doppler features of OTFS signals, our design can achieve accurate estimations of target position and velocity.
2) We develop an innovative approach to concurrently perform data association and target sensing tasks by formulating a mixed-integer optimization problem, which is efficiently solved with a polynomial complexity by approximated as a convex problem.
3) To enhance sensing performance, we propose an MLE-based method to address measurement errors, improving target state estimation based on target-measurement association.
4) Extensive simulations are performed, and comprehensive results validate the effectiveness of the proposed target sensing algorithm.

The remainder of this article is organized as follows. The preliminary study on OTFS-based sensing is introduced in Section II. The proposed MTAP method is discussed in Section III. Section IV expresses the developed MLE-based sensing approach, followed by the complexity analysis in Section V. Performance evaluation is conducted in Section VI, with the conclusion presented in Section VII.

Notations: Unless specific otherwise, vectors and matrices are denoted by boldface lowercase letters and uppercase letters, respectively. x^o and x^* are the true value and conjugate of x, respectively. $\|\mathbf{x}\|$ stands for the ℓ_2-norm of vector $\mathbf{x}$. $\mathbf{X}^{\mathrm{T}}$ and $\mathbf{X}^{-1}$ indicate the transpose and inverse, respectively. $\delta(\cdot)$ depicts the Dirac delta function, $\sum_{k=1}^{n} x_k$ is the sum of $x_1, x_2, \ldots, x_n$, and diag($\mathbf{x}$) represents the diagonal matrix with the elements of vector $\mathbf{x}$ on its diagonal. ∇f is the gradient of f and $\partial \mathbf{a}/\partial \mathbf{b}$ means partial derivative of $\mathbf{a}$ with respect to $\mathbf{b}$. $\mathbb{R}^n$ denotes the space of n-dimensional real vectors. Table I provides key symbols and notations adopted in this work.

II. PRELIMINARY

A. Scenario

We consider a typical distributed OTFS radar system, as illustrated in Fig. 1, consisting of N_t single-antenna transmitters and N_r single-antenna receivers. The known positions of each transmitter and receiver are denoted by $\mathbf{q}_i \in \mathbb{R}^d$ and $\mathbf{p}_j \in \mathbb{R}^d$, respectively, where $i = 1, 2, \ldots, N_t$ and $j = 1, 2, \ldots, N_r$. During data association, the emitted OTFS signals from the transmitters are reflected by the K moving targets (scatters) before being observed by the receivers. The unknown positions and velocities of the targets are denoted by $\mathbf{s}_k \in \mathbb{R}^d$ and $\dot{\mathbf{s}}_k \in \mathbb{R}^d$, respectively, $k = 1, 2, \ldots, K$.

The objective of this work is to develop an effective solution for the MTAP that arises in distributed OTFS radar systems. The challenge arises from the lack of knowledge of the receivers regarding the association between the targets and the extracted measurements, compounded by the simultaneous reflections from multiple targets.

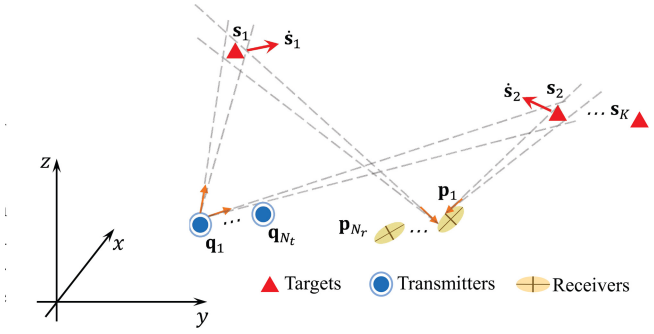

Fig. 1. Moving multitarget sensing scenario: determining the scatter positions $\mathbf{s}_1, \ldots, \mathbf{s}_K$ and velocities $\dot{\mathbf{s}}_1, \ldots, \dot{\mathbf{s}}_K$ based on transmitted and received OTFS signals.

B. OTFS Transceiver Structure

In this section, we introduce an OTFS communication system [18], with total bandwidth $B = M\Delta f$ and latency $T_f = NT$, where Δf represents the subcarrier space, and T is the symbol duration. Information bits are mapped to a NM symbol set in DD domain, i.e., $X_{DD}[k_u, l_u]$, where $0 \le k_u \le N-1$ and $0 \le l_u \le M-1$ stand for the indices of delay and Doppler shifts, respectively, and X_{DD} belongs to a constellation set $\mathcal{A}$. These DD domain symbols $X_{DD}[k_u, l_u]$ are transformed to the TF domain as $X_{TF}[n, m]$ through inverse symplectic finite Fourier transform (ISFFT), given by

$$X_{TF}[n,m] = \frac{1}{\sqrt{MN}} \sum_{k_u=0}^{N-1} \sum_{l_u=0}^{M-1} X_{DD}[k_u, l_u] e^{j2\pi\left(\frac{nk_u}{N} - \frac{ml_u}{M}\right)} \quad (1)$$

where $0 \le n \le N-1$ and $0 \le m \le M-1$ denote the indices for time and subcarrier, respectively. Subsequently, the TF domain symbols are mapped into a continuous time-domain signal via a multicarrier modulator, which is

$$s(t) = \sum_{m=0} \sum_{n=0} X_{TF}[n,m]\ e^{j2\pi m\Delta_f(t-nT)} g_{\text{tx}}(t-nT) \quad (2)$$

where $g_{\text{tx}}(t-nT)$ is the transmitter pulse shaping filter.

The signal $s(t)$ propagates over a multipath time-varying channel and is reflected by sensing targets, yielding the received signal $r(t)$ as

$$r(t) = \iint h(\tau, \nu) e^{j2\pi\nu(t-\tau)} s(t-\tau) d\tau d\nu + \omega(t) \quad (3)$$

where $\omega(t)$ is the AWGN process with power spectral density (PSD) N_0, and $h(\tau, \nu)$ is complex baseband channel impulse response, representing the channel's response to an impulse with delay τ and Doppler-shift ν. The $h(\tau, \nu)$ can be written as

$$h(\tau, \nu) = \sum_{i_p=1}^{P} h_{i_p} \delta(\tau - \tau_{i_p}) \delta(\nu - \nu_{i_p}) \quad (4)$$

where P is the number of resolvable reflectors. h_{i_p}, τ_{i_p} and ν_{i_p} represent the channel gain, delay and Doppler of the i_p-th path, respectively. Each transmitter-receiver pair has a total of K reflective paths.

Next, the TF domain received symbol $Y_{\text{TF}}[n, m]$ can be obtained by operating the Wigner transform on $r(t)$ [31], as

$$Y_{\text{TF}}[n,m] = \int_{-\infty}^{\infty} r(t) g_{rx}^*(t-nT)\ e^{-j2\pi m\Delta f(t-nT)} dt \quad (5)$$

where $g_{rx}(t)$ is the receiver pulse shaping filter. Then, the TF domain symbol $Y_{\text{TF}}[n, m]$ is transformed to the DD domain by performing symplectic finite Fourier transform (SFFT), which is

$$Y_{DD}[k_u, l_u] = \frac{1}{\sqrt{NM}} \sum_{n=0}^{N-1} \sum_{m=0}^{M-1} Y_{TF}[n,m]\ e^{-j2\pi\left(\frac{k_u n}{N} - \frac{l_u m}{M}\right)}. \quad (6)$$

Building on the above, the DD domain input-output relationship can be expressed as

$$Y_{DD}[k_u, l_u] = \sum_{k'_u=0}^{N-1} \sum_{l'_u=0}^{M-1} X_{DD}[k'_u, l'_u] h_w[(k_u - k'_u)_N, (l_u - l'_u)_M] + \omega[k_u, l_u] \quad (7)$$

where $h_w[k_u, l_u]$ denotes the DD domain effective channel, and $\omega[k_u, l_u]$ represents effective noise in the DD domain that is a Gaussian noise term with zero-mean PSD N_0.

The moving multitarget sensing scenario and OTFS transceiver structure have been detailed. In the next, we will formulate the problem and discuss the condition for the resolution.

C. Problem Formulation

Upon receiving OTFS signals, one can facilitate sensing tasks by exploiting the embedded delay and Doppler information. With a complex baseband channel impulse response $h(\tau, \nu)$ in (4), the range and relative velocity associated with i_p-th target are defined as r_{i_p} and $\dot{r}_{i_p}$, then the round-trip delay τ_{i_p} and the Doppler-shift ν_{i_p} can be expressed as

$$\tau_{i_p} = \frac{2r_{i_p}}{c} = \frac{l_{i_p}}{M\Delta f} \quad (8a)$$

$$\nu_{i_p} = \frac{2f_c\dot{r}_{i_p}}{c} = \frac{k_{i_p}}{NT} \quad (8b)$$

with c denoting the speed of light, and f_c the carrier frequency. As observed, the range and velocity can be determined as functions of k_{i_p} and l_{i_p}. To achieve that, a variety of methods with reliable performance have been developed, approaching Cramér-Rao Lower Bound (CRLB), e.g., embedding a superimposed pilot [20], 2-D correlation-based estimator [31] and difference-based method. Among them, 2-D correlation-based estimator is employed in this work for channel estimation. Finally, one can determine r_{i_p} and $\dot{r}_{i_p}$ based on (8a) and (8b) and the estimated k_{i_p} and l_{i_p} from channel estimation.

Take the kth target as a study case, the bistatic range (BR) for the (i, j)th transmitter-receiver pair can be modeled as

$$r_{ij}^k = \|\mathbf{q}_i - \mathbf{s}_k\| + \|\mathbf{p}_j - \mathbf{s}_k\| + n_{r,ij}^k \quad (9)$$

where $n_{r,ij}^k$ is the noise. The related range rate (RR) is defined as

$$\dot{r}_{ij}^k = \frac{(\mathbf{s}_k - \mathbf{q}_i)^{\text{T}}}{\|\mathbf{s}_k - \mathbf{q}_i\|} \dot{\mathbf{s}}_k + \frac{(\mathbf{s}_k - \mathbf{p}_j)^{\text{T}}}{\|\mathbf{s}_k - \mathbf{p}_j\|} \dot{\mathbf{s}}_k + n_{\dot{r},ij}^k \quad (10)$$

where $n^k_{\dot{r},ij}$ is the noise. Note that, the noise in both BR and RR noise follows zero-mean Gaussian distributions with known covariance.

Due to the orthogonality of OTFS signals, the distinction between BR and RR measurements from different transmitters can be made unambiguously. Furthermore, the BR and its corresponding RR measurement are derived from the same symbol, thus a direct mapping between them is established. In particular, the BR and RR measurements from the jth receiver can be organized in the data fusion center as

$$\mathbf{r}_j = \left[\mathbf{r}_{1j}^{\mathrm{T}}, \mathbf{r}_{2j}^{\mathrm{T}}, \ldots, \mathbf{r}_{N_t j}^{\mathrm{T}}\right]^{\mathrm{T}} \tag{11a}$$

$$\dot{\mathbf{r}}_j = \left[\dot{\mathbf{r}}_{1j}^{\mathrm{T}}, \dot{\mathbf{r}}_{2j}^{\mathrm{T}}, \ldots, \dot{\mathbf{r}}_{N_t j}^{\mathrm{T}}\right]^{\mathrm{T}} \tag{11b}$$

where $\mathbf{r}_{ij} = [r_{ij}^1, r_{ij}^2, \ldots, r_{ij}^K]^{\mathrm{T}}$ and $\dot{\mathbf{r}}_{ij} = [\dot{r}_{ij}^1, \dot{r}_{ij}^2, \ldots, \dot{r}_{ij}^K]^{\mathrm{T}}$ consist of K BR and RR measurements, respectively, arranged in the same specific order. For reliable sensing performance, the entries of $\mathbf{r}_{ij}$ and $\dot{\mathbf{r}}_{ij}$ need to be rearranged, so that the kth entries in the rearranged measurement sets correspond to a specific target, such as the target located at $\mathbf{s}_{u_k}$ with velocity $\dot{\mathbf{s}}_{u_k}$, where $u_k \in \{1, 2, \ldots, K\}$. With the measurements sets from the above equations, the permuted BR and RR measurement vector $\tilde{\mathbf{r}}_j$ and $\tilde{\dot{\mathbf{r}}}_j$ are

$$\tilde{\mathbf{r}}_j = \left[\tilde{\mathbf{r}}_{1j}^{\mathrm{T}}, \tilde{\mathbf{r}}_{2j}^{\mathrm{T}}, \ldots, \tilde{\mathbf{r}}_{N_t j}^{\mathrm{T}}\right]^{\mathrm{T}} \triangleq \mathbf{G}_j \mathbf{r}_j \tag{12a}$$

$$\tilde{\dot{\mathbf{r}}}_j = \left[\tilde{\dot{\mathbf{r}}}_{1j}^{\mathrm{T}}, \tilde{\dot{\mathbf{r}}}_{2j}^{\mathrm{T}}, \ldots, \tilde{\dot{\mathbf{r}}}_{N_t j}^{\mathrm{T}}\right]^{\mathrm{T}} \triangleq \mathbf{G}_j \dot{\mathbf{r}}_j \tag{12b}$$

where $\mathbf{G}_j$ is the permutation matrix that rearranges the observed measurements at each receiver j. This matrix ensures that the measurements from different targets are aligned, thus guaranteeing accurate estimation of the targets' positions and velocities.

To achieve accurate sensing, the kth entry of both $\tilde{\mathbf{r}}_{ij}$ and $\tilde{\dot{\mathbf{r}}}_{ij}$ is intended to correspond to the same target. Toward this end, we first partition the permutation matrix $\mathbf{G}_j$ as

$$\mathbf{G}_j = \mathrm{blkdiag}\big(\mathbf{G}_{1j}, \mathbf{G}_{2j}, \ldots, \mathbf{G}_{N_t j}\big) \tag{13}$$

where $\mathbf{G}_{ij}$'s is the permutation matrix with $\tilde{\mathbf{r}}_{ij} = \mathbf{G}_{ij}\mathbf{r}_{ij}$ and $\tilde{\dot{\mathbf{r}}}_{ij} = \mathbf{G}_{ij}\dot{\mathbf{r}}_{ij}$. To solve the MTAP, the goal is to determine the permutation matrix $\mathbf{G}_j$ that correctly arranges the collected measurements.

Before addressing the solution to the MTAP, we first discuss the minimum number of transmitters and receivers required for its resolution. For position and velocity estimation, the number of scalar unknowns is set to $Kd+Kd$. With the BR and RR measurements, the total number of scalar measurements is $N_tN_rK + N_tN_rK$. The MTAP is solvable only if the following condition is satisfied, which is

$$2N_tN_rK \geq 2Kd \tag{14}$$

where N_t and N_r are the numbers of transmitters and receivers, respectively. The position estimation problem is subject to reflection and rotation ambiguities, which can distort the results. However, these ambiguities can be resolved by utilizing BR measurements. Specifically, to ensure a unique intersection and accurate position estimation, the number of transmitters and receivers must satisfy the condition $N_tN_r \geq 3$. The minimum number of required transmitters and receivers is summarized as

$$\begin{cases} N_tNr \geq 3, & \text{if} \quad d = 2 \\ N_tNr \geq d, & \text{if} \quad d \geq 3. \end{cases} \tag{15}$$

After formulating the problem and discussing the conditions for its solution, we will introduce a convex solution for MTAP in the next section.

III. Convex Solution for MTAP

In this section, we propose a novel method to address the MTAP issue stated in Section II-C, by determining the permutation matrices $\mathbf{G}_j$'s, each of which aligns the observed measurements at receiver j with their corresponding targets, thereby resolving the underlying association ambiguity in distributed OTFS radar systems. To achieve this, we define the BR and RR measurement permutation error as

$$e_{ij}^k \triangleq \mathbf{g}_j^z \mathbf{r}_j - \left(\left\|\mathbf{q}_i - \mathbf{s}_{u_k}\right\| + \left\|\mathbf{p}_j - \mathbf{s}_{u_k}\right\|\right) \tag{16a}$$

$$\dot{e}_{ij}^k \triangleq \mathbf{g}_j^z \dot{\mathbf{r}}_j - \left(\frac{\left(\mathbf{s}_{u_k} - \mathbf{q}_i\right)^{\mathrm{T}}}{\left\|\mathbf{s}_{u_k} - \mathbf{q}_i\right\|}\dot{\mathbf{s}}_{u_k} + \frac{\left(\mathbf{s}_{u_k} - \mathbf{p}_j\right)^{\mathrm{T}}}{\left\|\mathbf{s}_{u_k} - \mathbf{p}_j\right\|}\dot{\mathbf{s}}_{u_k}\right) \tag{16b}$$

where $z = k + K(i-1)$ denotes the zth row of the $\mathbf{G}_j$. Note that, the errors will be zero if the measurements are correctly permuted in the absence of noise. The permutation matrix $\mathbf{G}_j$ can be obtained through solving

$$\underset{\mathbf{s}_{u_k}, \dot{\mathbf{s}}_{u_k}, \mathbf{G}_j}{\text{minimize}} \quad \sum_{j=1}^{N_r}\sum_{i=1}^{N_t}\sum_{k=1}^{K}\left(\left(e_{ij}^k\right)^2 + \left(\dot{e}_{ij}^k\right)^2\right). \tag{17}$$

However, the above equation is a nonconvex problem, which is challenging to solve directly. To address this, the auxiliary variables d_{ij}^k and $\dot{d}_{ij}^k$ are introduced, then (17) can be represented as

$$\underset{\mathbf{s}_{u_k}, \dot{\mathbf{s}}_{u_k}, \mathbf{G}_j, d_{ij}^k, \dot{d}_{ij}^k}{\text{minimize}} \quad \sum_{j=1}^{N_r}\sum_{i=1}^{N_t}\sum_{k=1}^{K}\left(\left(d_{ij}^k\right)^2 + \left(\dot{d}_{ij}^k\right)^2\right) \tag{18a}$$

$$\text{s.t.} \quad \mathbf{g}_j^k \mathbf{r}_j - \left\|\mathbf{q}_i - \mathbf{s}_{u_k}\right\| - \left\|\mathbf{s}_{u_k} - \mathbf{p}_j\right\| \leq d_{ij}^k \tag{18b}$$

$$\mathbf{g}_j^k \mathbf{r}_j - \left\|\mathbf{q}_i - \mathbf{s}_{u_k}\right\| - \left\|\mathbf{s}_{u_k} - \mathbf{p}_j\right\| \geq -d_{ij}^k \tag{18c}$$

$$\mathbf{g}_j^k \dot{\mathbf{r}}_j - \frac{\left(\mathbf{s}_{u_k} - \mathbf{q}_i\right)^{\mathrm{T}}}{\left\|\mathbf{s}_{u_k} - \mathbf{q}_i\right\|}\dot{\mathbf{s}}_{u_k} - \frac{\left(\mathbf{s}_{u_k} - \mathbf{p}_j\right)^{\mathrm{T}}}{\left\|\mathbf{s}_{u_k} - \mathbf{p}_j\right\|}\dot{\mathbf{s}}_{u_k} \leq \dot{d}_{ij}^k \tag{18d}$$

$$\mathbf{g}_j^k \dot{\mathbf{r}}_j - \frac{\left(\mathbf{s}_{u_k} - \mathbf{q}_i\right)^{\mathrm{T}}}{\left\|\mathbf{s}_{u_k} - \mathbf{q}_i\right\|}\dot{\mathbf{s}}_{u_k} - \frac{\left(\mathbf{s}_{u_k} - \mathbf{p}_j\right)^{\mathrm{T}}}{\left\|\mathbf{s}_{u_k} - \mathbf{p}_j\right\|}\dot{\mathbf{s}}_{u_k} \geq -\dot{d}_{ij}^k. \tag{18e}$$

Since these permutation matrices rearrange the places of measured vectors only, their entries should be either 0 or 1. Under this condition, problem (18) can be categorized as a mixed-integer program, making it difficult to obtain a global-optimal solution. For that, we relax the conditions necessary but not sufficient, by

$$0 \leq g_{ij}^{lu} \leq 1, \quad \sum_{l=1}^{K} g_{ij}^{lu} = 1, \quad \sum_{u=1}^{K} g_{ij}^{lu} = 1 \tag{19}$$

where g_{ij}^{lu} is the (l, u)th entry of $\mathbf{G}_{ij}$. Having these relaxed conditions, (18) can be transformed into

$$\underset{\mathbf{s}_{u_k},\dot{\mathbf{s}}_{u_k},\mathbf{G}_{ij},d_{ij}^k,\dot{d}_{ij}^k}{\text{minimize}} \quad \sum_{j=1}^{N_r}\sum_{i=1}^{N_t}\sum_{k=1}^{K}\left(\left(d_{ij}^k\right)^2+\left(\dot{d}_{ij}^k\right)^2\right) \tag{20a}$$

$$\text{s.t.} \quad \mathbf{g}_{ij}^k\mathbf{r}_j-\left\|\mathbf{q}_i-\mathbf{s}_{u_k}\right\|-\left\|\mathbf{s}_{u_k}-\mathbf{p}_j\right\|\le d_{ij}^k \tag{20b}$$

$$\mathbf{g}_{ij}^k\mathbf{r}_j-\left\|\mathbf{q}_i-\mathbf{s}_{u_k}\right\|-\left\|\mathbf{s}_{u_k}-\mathbf{p}_j\right\|\ge -d_{ij}^k \tag{20c}$$

$$\mathbf{g}_{ij}^k\dot{\mathbf{r}}_j-\frac{\left(\mathbf{s}_{u_k}-\mathbf{q}_i\right)^{\mathrm{T}}}{\left\|\mathbf{s}_{u_k}-\mathbf{q}_i\right\|}\dot{\mathbf{s}}_{u_k}-\frac{\left(\mathbf{s}_{u_k}-\mathbf{p}_j\right)^{\mathrm{T}}}{\left\|\mathbf{s}_{u_k}-\mathbf{p}_j\right\|}\dot{\mathbf{s}}_{u_k}\le \dot{d}_{ij}^k \tag{20d}$$

$$\mathbf{g}_{ij}^k\dot{\mathbf{r}}_j-\frac{\left(\mathbf{s}_{u_k}-\mathbf{q}_i\right)^{\mathrm{T}}}{\left\|\mathbf{s}_{u_k}-\mathbf{q}_i\right\|}\dot{\mathbf{s}}_{u_k}-\frac{\left(\mathbf{s}_{u_k}-\mathbf{p}_j\right)^{\mathrm{T}}}{\left\|\mathbf{s}_{u_k}-\mathbf{p}_j\right\|}\dot{\mathbf{s}}_{u_k}\ge -\dot{d}_{ij}^k \tag{20e}$$

$$0\le g_{ij}^{lu}\le 1,\quad \sum_{l=1}^{K}g_{ij}^{lu}=1,\quad \sum_{u=1}^{K}g_{ij}^{lu}=1 \tag{20f}$$

where $\mathbf{g}_{ij}^k$ denotes the kth row of $\mathbf{G}_{ij}$.

Now, the problem in (20) only contains continuous variables. However, addressing the problem in (20) is still challenging due to the nonconvex constraints in (20b), (20d) and (20e). To tackle this problem, we apply the first-order Taylor approximation. Specifically, we define the following functions as

$$f_{ij}(\mathbf{x})\triangleq \|\mathbf{q}_i-\mathbf{x}\|+\left\|\mathbf{x}-\mathbf{p}_j\right\| \tag{21a}$$

$$h_{ij}(\mathbf{x},\mathbf{y})\triangleq \frac{\left(\mathbf{x}-\mathbf{q}_i\right)^{\mathrm{T}}}{\left\|\mathbf{x}-\mathbf{q}_i\right\|}\mathbf{y}+\frac{\left(\mathbf{x}-\mathbf{p}_j\right)^{\mathrm{T}}}{\left\|\mathbf{x}-\mathbf{p}_j\right\|}\mathbf{y}. \tag{21b}$$

Then, the first-order Taylor approximation of $f_{ij}(\mathbf{x})$ at point $\mathbf{s}_{u_k}^{(n)}$ can be obtained by

$$f_{i,j}(\mathbf{x})\cong f_{i,j}\left(\mathbf{s}_{u_k}^{(n)}\right)+\nabla_{\mathbf{x}}f_{i,j}\left(\mathbf{s}_{u_k}^{(n)}\right)\left(\mathbf{x}-\mathbf{s}_{u_k}^{(n)}\right) \tag{22}$$

where $\nabla_{\mathbf{x}}f_{i,j}(\mathbf{s}_{u_k}^{(n)})$ is the gradient of $f_{i,j}(\mathbf{x})$ evaluated at $\mathbf{s}_{u_k}^{(n)}$, which is

$$\nabla_{\mathbf{x}}f_{i,j}\left(\mathbf{s}_{u_k}^{(n)}\right)=\frac{\left(\mathbf{s}_{u_k}^{(n)}-\mathbf{q}_i\right)^{\mathrm{T}}}{\left\|\mathbf{s}_{u_k}^{(n)}-\mathbf{q}_i\right\|}+\frac{\left(\mathbf{s}_{u_k}^{(n)}-\mathbf{p}_j\right)^{\mathrm{T}}}{\left\|\mathbf{s}_{u_k}^{(n)}-\mathbf{p}_j\right\|}. \tag{23}$$

Similarly, the first-order Taylor approximation of $h_{ij}(\mathbf{x},\mathbf{y})$ at point $(\mathbf{s}_{u_k}^{(n)},\dot{\mathbf{s}}_{u_k}^{(n)})$ can be written as

$$\begin{aligned}h_{i,j}(\mathbf{x},\mathbf{y})\cong\ & h_{i,j}\left(\mathbf{s}_{u_k}^{(n)},\dot{\mathbf{s}}_{u_k}^{(n)}\right)+\nabla_{\mathbf{x}}h_{i,j}\left(\mathbf{s}_{u_k}^{(n)},\dot{\mathbf{s}}_{u_k}^{(n)}\right)\left(\mathbf{x}-\mathbf{s}_{u_k}^{(n)}\right)\\&+\nabla_{\mathbf{y}}h_{i,j}\left(\mathbf{s}_{u_k}^{(n)},\dot{\mathbf{s}}_{u_k}^{(n)}\right)\left(\mathbf{y}-\dot{\mathbf{s}}_{u_k}^{(n)}\right)\end{aligned} \tag{24}$$

where

$$\begin{aligned}&\nabla_{\mathbf{x}}h_{i,j}\left(\mathbf{s}_{u_k}^{(n)},\dot{\mathbf{s}}_{u_k}^{(n)}\right)\\&=\frac{\left(\dot{\mathbf{s}}_{u_k}^{(n)}\right)^{\mathrm{T}}}{\left\|\mathbf{s}_{u_k}^{(n)}-\mathbf{q}_i\right\|}-\frac{\left(\mathbf{s}_{u_k}^{(n)}-\mathbf{q}_i\right)^{\mathrm{T}}\dot{\mathbf{s}}_{u_k}^{(n)}\left(\mathbf{s}_{u_k}^{(n)}-\mathbf{q}_i\right)^{\mathrm{T}}}{\left\|\mathbf{s}_{u_k}^{(n)}-\mathbf{q}_i\right\|^3}\\&+\frac{\left(\dot{\mathbf{s}}_{u_k}^{(n)}\right)^{\mathrm{T}}}{\left\|\mathbf{s}_{u_k}^{(n)}-\mathbf{p}_j\right\|}-\frac{\left(\mathbf{s}_{u_k}^{(n)}-\mathbf{p}_j\right)^{\mathrm{T}}\dot{\mathbf{s}}_{u_k}^{(n)}\left(\mathbf{s}_{u_k}^{(n)}-\mathbf{p}_j\right)^{\mathrm{T}}}{\left\|\mathbf{s}_{u_k}^{(n)}-\mathbf{p}_j\right\|^3}\end{aligned} \tag{25}$$

and

$$\nabla_{\mathbf{y}}h_{i,j}\left(\mathbf{s}_{u_k}^{(n)},\dot{\mathbf{s}}_{u_k}^{(n)}\right)=\frac{\left(\mathbf{s}_{u_k}^{(n)}-\mathbf{q}_i\right)^{\mathrm{T}}}{\left\|\mathbf{s}_{u_k}^{(n)}-\mathbf{q}_i\right\|}+\frac{\left(\mathbf{s}_{u_k}^{(n)}-\mathbf{p}_j\right)^{\mathrm{T}}}{\left\|\mathbf{s}_{u_k}^{(n)}-\mathbf{p}_j\right\|}. \tag{26}$$

Considering the fact that the nonconvex constraint (20b), (20d) and (20e) can be written as $\mathbf{g}_{ij}^k\mathbf{r}_j-f_{i,j}(\mathbf{s}_{u_k})\ge -d_{ij}^k$, $\mathbf{g}_{ij}^k\dot{\mathbf{r}}_j-h_{i,j}(\mathbf{s}_{u_k},\dot{\mathbf{s}}_{u_k})\le -\dot{d}_{ij}^k$, and $\mathbf{g}_{ij}^k\dot{\mathbf{r}}_j-h_{i,j}(\mathbf{s}_{u_k},\dot{\mathbf{s}}_{u_k})\ge -\dot{d}_{ij}^k$, substituting (22) and (24) into these nonconvex constraints (20b), (20d) and (20e), the problem (20) can re-expressed as

$$\underset{\mathbf{s}_{u_k},\dot{\mathbf{s}}_{u_k},\mathbf{G}_{ij},d_{ij}^k,\dot{d}_{ij}^k}{\text{minimize}} \quad \sum_{j=1}^{N_r}\sum_{i=1}^{N_t}\sum_{k=1}^{K}\left(\left(d_{ij}^k\right)^2+\left(\dot{d}_{ij}^k\right)^2\right) \tag{27a}$$

$$\begin{aligned}\text{s.t.}\quad & \mathbf{g}_{ij}^k\mathbf{r}_j-f_{i,j}\left(\mathbf{s}_{u_k}^{(n)}\right)\\&-\nabla_{\mathbf{x}}f_{i,j}\left(\mathbf{s}_{u_k}^{(n)}\right)\left(\mathbf{s}_{u_k}-\mathbf{s}_{u_k}^{(n)}\right)\le d_{ij}^k\end{aligned} \tag{27b}$$

$$\mathbf{g}_{ij}^k\mathbf{r}_j-f_{i,j}(\mathbf{s}_{u_k})\ge -d_{ij}^k \tag{27c}$$

$$\begin{aligned}&\mathbf{g}_{ij}^k\dot{\mathbf{r}}_j-h_{i,j}\left(\mathbf{s}_{u_k}^{(n)},\dot{\mathbf{s}}_{u_k}^{(n)}\right)\\&-\nabla_{\mathbf{x}}h_{i,j}\left(\mathbf{s}_{u_k}^{(n)},\dot{\mathbf{s}}_{u_k}^{(n)}\right)\left(\mathbf{s}_{u_k}-\mathbf{s}_{u_k}^{(n)}\right)\\&-\nabla_{\mathbf{y}}h_{i,j}\left(\mathbf{s}_{u_k}^{(n)},\dot{\mathbf{s}}_{u_k}^{(n)}\right)\left(\dot{\mathbf{s}}_{u_k}-\dot{\mathbf{s}}_{u_k}^{(n)}\right)\le \dot{d}_{ij}^k\end{aligned} \tag{27d}$$

$$\begin{aligned}&\mathbf{g}_{ij}^k\dot{\mathbf{r}}_j-h_{i,j}\left(\mathbf{s}_{u_k}^{(n)},\dot{\mathbf{s}}_{u_k}^{(n)}\right)\\&-\nabla_{\mathbf{x}}h_{i,j}\left(\mathbf{s}_{u_k}^{(n)},\dot{\mathbf{s}}_{u_k}^{(n)}\right)\left(\mathbf{s}_{u_k}-\mathbf{s}_{u_k}^{(n)}\right)\\&-\nabla_{\mathbf{y}}h_{i,j}\left(\mathbf{s}_{u_k}^{(n)},\dot{\mathbf{s}}_{u_k}^{(n)}\right)\left(\dot{\mathbf{s}}_{u_k}-\dot{\mathbf{s}}_{u_k}^{(n)}\right)\ge -\dot{d}_{ij}^k\end{aligned} \tag{27e}$$

$$0\le g_{ij}^{lu}\le 1,\quad \sum_{l=1}^{K}g_{ij}^{lu}=1,\quad \sum_{u=1}^{K}g_{ij}^{lu}=1. \tag{27f}$$

Following the above steps, the problem in (18) is converted to a convex optimization problem, which can be efficiently solved using the CVX toolbox in the MATLAB environment. Both the permutation matrices and target state are estimated by addressing (27). However, the Taylor approximation in (27) may induce errors in the subsequent steps, potentially degrading system performance. Given this issue, we update the Taylor approximations (22) and (24) based on the previous estimates of $\mathbf{s}_{u_k}$ and $\mathbf{B}_{u_k}$, which are denoted by $\mathbf{s}_{u_k}^{(n+1)}$ and $\mathbf{B}_{u_k}^{(n+1)}$, thereby enhancing estimation accuracy. This step is repeated until the convergence conditions are met. The procedure of the proposed method is illustrated in Algorithm 1.

Remark 1: Note that the initial points $\mathbf{s}_{u_1}^{(0)}$, $\mathbf{s}_{u_2}^{(0)}$, …, $\mathbf{s}_{u_K}^{(0)}$ must be chosen to avoid close proximity to the positions of transmitters or receivers. This is because the absolute values of the gradients $\nabla_{\mathbf{x}}f_{i,j}(\mathbf{s}_{u_k}^{(n)})$ and $\nabla_{\mathbf{x}}h_{i,j}(\mathbf{s}_{u_k}^{(n)},\dot{\mathbf{s}}_{u_k}^{(n)})$ will be significantly larger and result in a huge error in first-order Taylor approximation if the $\mathbf{s}_{u_k}^{(0)}$ approaches $\mathbf{q}_i$ or $\mathbf{p}_j$, leading to local convergence or even divergence.

As discussed earlier, the matrices $\hat{\mathbf{G}}_{ij}$'s represent the estimated permutation matrices rather than their exact forms. The exact estimates of $\mathbf{G}_{ij}$ can be obtained by applying the general rounding rule, assigning entries to 0 or 1 based on their respective values. However, if all elements in a row or

Algorithm 1 Solution for MTAP

Input: $\{\mathbf{r}_j\}$ - Measured N_rN_tK BRs.
$\{\dot{\mathbf{r}}_j\}$ - Measured N_rN_tK RRs.
Condition: $N_tN_r \geq d$.
Implementation:
1) Initialize $\mathbf{s}_{u_1}^{(0)}$, $\mathbf{s}_{u_2}^{(0)}$, …, $\mathbf{s}_{u_K}^{(0)}$ and $\dot{\mathbf{s}}_{u_1}^{(0)}$, $\dot{\mathbf{s}}_{u_2}^{(0)}$, …, $\dot{\mathbf{s}}_{u_K}^{(0)}$.
2) Set the threshold ξ and $\dot{\xi}$.
3) Set $n \longleftarrow 0$.
4) **While** $\sum_{k=1}^{K}\left\|\mathbf{s}_{u_k}^{(n)}-\mathbf{s}_{u_k}^{(n-1)}\right\|_2^2 > \xi$ **or** $\sum_{k=1}^{K}\left\|\dot{\mathbf{s}}_{u_k}^{(n)}-\dot{\mathbf{s}}_{u_k}^{(n-1)}\right\|_2^2 > \dot{\xi}$ **do**.
5) Update $f_{i,j}\left(\mathbf{s}_{u_k}^{(n)}\right)$ in (22), $\nabla_{\mathbf{x}} f_{i,j}\left(\mathbf{s}_{u_k}^{(n)}\right)$ in (23), $h_{i,j}\left(\mathbf{s}_{u_k}^{(n)}, \dot{\mathbf{s}}_{u_k}^{(n)}\right)$ in (24), $\nabla_{\mathbf{x}} h_{i,j}\left(\mathbf{s}_{u_k}^{(n)}, \dot{\mathbf{s}}_{u_k}^{(n)}\right)$ in (25) and $\nabla_{\mathbf{y}} h_{i,j}\left(\mathbf{s}_{u_k}^{(n)}, \dot{\mathbf{s}}_{u_k}^{(n)}\right)$ in (26).
6) Solve (27) to obtain the solutions $\mathbf{G}_{ij}$'s, $\mathbf{s}_{u_k}^{(n+1)}$'s and $\dot{\mathbf{s}}_{u_k}^{(n+1)}$'s.
7) $n \longleftarrow n+1$.
8) **End while**
Output: $\mathbf{G}_{ij}$'s - Estimates of permutation matrices.
$\hat{\mathbf{s}}_{u_k}$'s and $\hat{\dot{\mathbf{s}}}_{u_k}$'s - Estimates of target states.

column are less than 0.5, this method becomes ineffective. To address this, specific convergence conditions should be taken into account, ensuring that at least one element greater than 0.5 in each row and column. Toward this end, we propose to employ another criterion to the permutation matrices, which is

$$\tilde{\mathbf{G}}_{ij} = \arg\max_{\mathbf{E}\in\mathcal{H}} \operatorname{trace}\left(\hat{\mathbf{G}}_{ij}^{\mathrm{T}}\mathbf{E}\right) \tag{28}$$

where $\mathcal{H}$ is the set of all possible $K \times K$ permutation matrices. Then, the exact estimates of permutation matrices $\mathbf{G}_j$'s can be obtained by

$$\tilde{\mathbf{G}}_j = \operatorname{blkdiag}\left(\tilde{\mathbf{G}}_{1j}, \tilde{\mathbf{G}}_{2j}, \ldots, \tilde{\mathbf{G}}_{N_tj}\right). \tag{29}$$

With the data associations resolved, the multitarget sensing problem is decomposed into K single-target sensing tasks. This problem can be addressed by using well-known estimation methods to estimate each target location and velocity based on the corresponding BB and BR measurements. It is noteworthy that although (27) provides estimates of $\mathbf{s}_{u_k}$ and $\dot{\mathbf{s}}_{u_k}$ along with the permutation matrices, these estimates exhibit low accuracy and may not reach the CRLB, particularly under high noise conditions. To enhance accuracy, we need to refine the preliminary solution in (27) to obtain more accurate estimations for $\mathbf{s}_{u_k}$'s and $\dot{\mathbf{s}}_{u_k}$'s, as detailed in the next section.

IV. Position and Velocity Estimation Refinement

As discussed previously, the preliminary MTAP solution is suboptimal due to relaxed constraints and ignored measurement noise. In this section, we propose an MLE to refine the solution using the permuted measurements.

Specifically, with the permuted measurements from the last section, all the BR and RR measurements are collected by the $N_tN_rK \times 1$ measurement vectors,

$$\mathbf{r} = \left[\mathbf{r}_1^{\mathrm{T}}, \mathbf{r}_1^{\mathrm{T}}, \ldots, \mathbf{r}_{N_r}^{\mathrm{T}}\right]^{\mathrm{T}} \tag{30a}$$

$$\dot{\mathbf{r}} = \left[\dot{\mathbf{r}}_1^{\mathrm{T}}, \dot{\mathbf{r}}_2^{\mathrm{T}}, \ldots, \dot{\mathbf{r}}_{N_r}^{\mathrm{T}}\right]^{\mathrm{T}}. \tag{30b}$$

The noise vectors corresponding to $\mathbf{r}$ and $\dot{\mathbf{r}}$ are denoted as $\mathbf{n}_{\mathbf{r}}$ and $\mathbf{n}_{\dot{\mathbf{r}}}$, respectively. Considering both the BR and RR measurements are uncorrelated zero-mean Gaussian noise with known covariance, the covariance matrices $\mathbf{Q}_{\mathbf{r}}$ of $\mathbf{n}_{\mathbf{r}}$ and $\mathbf{Q}_{\dot{\mathbf{r}}}$ of $\mathbf{n}_{\dot{\mathbf{r}}}$ shall be known. The quantities we aim to estimate are the target positions and velocities,

$$\mathbf{S} = [\mathbf{s}_1, \mathbf{s}_2, \ldots, \mathbf{s}_K] \tag{31a}$$

$$\dot{\mathbf{S}} = [\dot{\mathbf{s}}_1, \dot{\mathbf{s}}_2, \ldots, \dot{\mathbf{s}}_K]. \tag{31b}$$

Under the Gaussian noise model, the MLE is

$$\begin{aligned}\left(\hat{\mathbf{S}}, \hat{\dot{\mathbf{S}}}\right) = \arg\min\Big\{&\left(\mathbf{r}-\mathbf{r}(\mathbf{S},\dot{\mathbf{S}})\right)^{\mathrm{T}}\mathbf{Q}_{\mathbf{r}}^{-1}\left(\mathbf{r}-\mathbf{r}(\mathbf{S},\dot{\mathbf{S}})\right)\\ &+\left(\dot{\mathbf{r}}-\dot{\mathbf{r}}(\mathbf{S},\dot{\mathbf{S}})\right)^{\mathrm{T}}\mathbf{Q}_{\dot{\mathbf{r}}}^{-1}\left(\dot{\mathbf{r}}-\dot{\mathbf{r}}(\mathbf{S},\dot{\mathbf{S}})\right)\Big\}\end{aligned} \tag{32}$$

where $\mathbf{r}(\mathbf{S},\dot{\mathbf{S}})$ and $\dot{\mathbf{r}}(\mathbf{S},\dot{\mathbf{S}})$ represent the parametric forms of the BRs and RRs in terms of the unknowns. Due to the high dimension of the unknown parameter space and the complicated error surface, it is infeasible to directly optimize MLE in (32) through grid search. However, the preliminary solution might provide adequate accuracy as the initial value for an iterative implementation of MLE to enhance precision.

For notation convenience, the unknowns of the target positions and velocities can be collected in the composite unknown vector, given by

$$\boldsymbol{\theta}^o = \left[\mathbf{s}_1^{oT}, \mathbf{s}_2^{oT}, \ldots, \mathbf{s}_K^{oT}, \dot{\mathbf{s}}_1^{oT}, \dot{\mathbf{s}}_2^{oT}, \ldots, \dot{\mathbf{s}}_K^{oT}\right]^{\mathrm{T}}. \tag{33}$$

In particular, we adopt the Gauss-Newton MLE for a highly accurate solution, which is

$$\begin{aligned}\hat{\boldsymbol{\theta}}^{(l+1)} = \hat{\boldsymbol{\theta}}^{(l)} &+ \left[\mathcal{B}^{(l)T}\mathbf{Q}^{-1}\mathcal{B}^{(l)}\right]^{-1}\\ &\times \mathcal{B}^{(l)T}\mathbf{Q}^{-1}\left[\mathbf{m}-\mathbf{m}\left(\boldsymbol{\theta}^{(l)}\right)\right]\end{aligned} \tag{34}$$

for $l = 0, 1, \ldots, L-1$.

In MLE, l is the iteration count, and L is the total iteration number. $\mathbf{Q} = \operatorname{blkdiag}(\mathbf{Q}_{\mathbf{r}}, \mathbf{Q}_{\dot{\mathbf{r}}})$, $\mathbf{m} = [\mathbf{r}^{\mathrm{T}}, \dot{\mathbf{r}}^{\mathrm{T}}]^{\mathrm{T}}$, $\mathbf{m}(\boldsymbol{\theta}^{(l)})$ represents the parametric forms of the BRs and RRs in terms of $\boldsymbol{\theta}^{(l)}$, and the initial value $\boldsymbol{\theta}^{(0)}$ is the preliminary solution from (27). The $2N_tN_rK \times 2Kd$ matrix $\mathcal{B}$ is the gradients of BRs and RRs with respect to the target positions and velocities. They are, from (9) and (10),

$$\frac{\partial \dot{r}_{ij}^{k_1}(\boldsymbol{\theta})}{\partial \mathbf{s}_{k_2}} = \frac{\partial \dot{r}_{ij}^{k_1}(\boldsymbol{\theta})}{\partial \dot{\mathbf{s}}_{k_2}} = \frac{\partial r_{ij}^{k_1}(\boldsymbol{\theta})}{\partial \mathbf{s}_{k_2}} = 0, \quad k_1 \neq k_2 \tag{35a}$$

$$\frac{\partial r_{ij}^{k}(\boldsymbol{\theta})}{\partial \mathbf{s}_k} = \boldsymbol{\rho}_{\mathbf{s}_k,\mathbf{q}_i} + \boldsymbol{\rho}_{\mathbf{s}_k,\mathbf{p}_j} \tag{35b}$$

$$\frac{\partial \dot{r}_{ij}^{k}(\boldsymbol{\theta})}{\partial \mathbf{s}_k} = \boldsymbol{\xi}_{\mathbf{s}_k,\mathbf{q}_i} + \boldsymbol{\xi}_{\mathbf{s}_k,\mathbf{p}_j} \tag{35c}$$

$$\frac{\partial \dot{r}_{ij}^{k}(\boldsymbol{\theta})}{\partial \dot{\mathbf{s}}_k} = \frac{\partial r_{ij}^{k}(\boldsymbol{\theta})}{\partial \mathbf{s}_k} \tag{35d}$$

where

$$\boldsymbol{\xi}_{\mathbf{s}_k^o,\mathbf{q}_i} = \frac{\dot{\mathbf{s}}_k}{\|\mathbf{s}_k - \mathbf{q}_i\|} - \frac{(\mathbf{s}_k - \mathbf{q}_i)^{\mathrm{T}}\dot{\mathbf{s}}_k}{\|\mathbf{s}_k - \mathbf{q}_i\|^2}\boldsymbol{\rho}_{\mathbf{s}_k,\mathbf{q}_i} \tag{36a}$$

$$\boldsymbol{\xi}_{\mathbf{s}_k^o,\mathbf{p}_j} = \frac{\dot{\mathbf{s}}_k}{\|\mathbf{s}_k - \mathbf{p}_j\|} - \frac{(\mathbf{s}_k - \mathbf{p}_j)^{\mathrm{T}}\dot{\mathbf{s}}_k}{\|\mathbf{s}_k - \mathbf{p}_j\|^2}\boldsymbol{\rho}_{\mathbf{s}_k,\mathbf{p}_j}. \tag{36b}$$

V. Complexity Analysis

In this section, we examine the computational complexities of the proposed data association algorithm and iterative MLE.

A. Data Association Algorithm

The data association algorithm progresses from (27) to (29), with the dominant complexity arising from (27), which can be written as second-order cone programming (SOCP). Consider the practical cases that $N_tN_r \gg 1$ and $K^2 \gg 1$, the corresponding computation complexity of solving the SOCP with precision ϵ using interior point methods is $\mathcal{O}(K^7(N_tN_r)^{3.5}\ln(1/\epsilon))$. Moreover, to obtain the valid permutation matrices in (28), we examine all possible permutation matrices with $K!N_tN_r$ in total, which requires a computational complexity of $\mathcal{O}(K!N_tN_r)$. Consequently, the complexity of the data association algorithm is

$$\mathcal{C}_{\mathrm{DA}} = \mathcal{O}\Big(K^7(N_tN_r)^{3.5}\ln(1/\epsilon) + K!N_tN_r\Big). \tag{37}$$

B. Iterative MLE

The iterative MLE in (34) has the complexity primarily determined by the computation and inversion of the matrix. The size of gradient matrix $\mathcal{B}$ is $2N_tN_rK \times 2Kd$. Assuming the matrix $\mathbf{Q}^{-1}$ has been calculated, the complexity to find the matrix for inversion is $\mathcal{O}(8K^3N_tN_rd(d + N_tN_r))$. The matrix inversion has the complexity of $\mathcal{O}((2Kd)^{\xi})$, where the parameter ξ is 3 typically and 2.376 by the Smith-Winograd algorithm. Given the iteration number of L_M, the total complexity of the iterative MLE is

$$\mathcal{C}_{\mathrm{MLE}} = \mathcal{O}\Big(L_M\Big(8K^3N_tN_rd(d + N_tN_r) + (2Kd)^{\xi}\Big)\Big). \tag{38}$$

In summary, the computational complexity of the data association and the iterative MLE are provided in (37) and (38), respectively. As observed, (37) gets a higher complexity than (38), primarily due to the computational demands of solving the SOCP in the data association algorithm. Therefore, the complexity of the localization process is dominated by the SOCP.

VI. Experiments and Evaluations

In this section, numerous simulations are performed to validate the effectiveness of the proposed work.

A. Setting

We consider an outdoor scenario for moving multitarget sensing, with The Cartesian coordinates of the actual parameters of transmitters, receivers, and targets demonstrated in Table II. We set signal propagation speed $c = 299792458$ m/s, No. of subcarriers $M = 64$, No. of OTFS symbols $N = 64$, carrier frequency $f_c = 4$ GHz, subcarrier spacing $\Delta f = 10$ KHz, transmitter gain $G_t = 55$ dB, and receiver gain $G_r = 55$ dB. The path loss $\rho_{i,j}^k$ between the (i, j) th transmitter-receiver for the $k-$th target is computed based on Friis' Law [32], given by

TABLE II
Parameters of Transmitters, Receivers and Targets

i	x_{q_i}(m)	y_{q_i}(m)	z_{q_i}(m)	j	x_{p_j}(m)	y_{p_j}(m)	z_{p_j}(m)
1	-400	-300	300	1	-500	-500	200
2	-400	300	200	2	500	500	100
3	400	300	50	3	0	800	200
4	200	700	400	4	800	0	100
5	-200	0	-400	5	-800	0	200
6	800	0	-200	6	-300	-350	150
k	x_{s_k}(m)	y_{s_k}(m)	z_{s_k}(m)	k	$\dot{x}_{s_k}$(m/s)	$\dot{y}_{s_k}$(m/s)	$\dot{z}_{s_k}$(m/s)
1	400	550	600	1	12	-5	20
2	-350	480	750	2	15	5	10
3	200	-300	800	3	15	-15	5
4	-450	-300	650	4	8	10	15
5	-100	450	950	5	-8	6	20
6	100	-250	750	6	10	8	-12

$$\rho_{i,j}^k = G_{\mathrm{r}}G_{\mathrm{t}}\left(\frac{\lambda_c}{4\pi r_{i,j}^k}\right)^2 \tag{39}$$

where $\lambda_c = c/f_c$ is the wavelength. The Cartesian coordinates of initial locations $\mathbf{s}_{u_k}^{(0)}$'s and velocities $\dot{\mathbf{s}}_{u_k}^{(0)}$ are selected randomly according in $x, y \sim \mathcal{U}(-700, 700)$m, $z \sim \mathcal{U}(500, 1000)$m, and $\dot{x}, \dot{y}, \dot{z} \sim \mathcal{U}(-30, 30)$m/s.

The root-mean-square error (RMSE) is selected as the performance metric, which is

$$\mathrm{RMSE}(\hat{*}) = \sqrt{\frac{1}{KL}\sum_{k=1}^{K}\sum_{l=1}^{L}\left\|(\hat{*})_{kl} - (*^o)_k\right\|^2} \tag{40}$$

where $(*^o)_k$ is the actual value of the position or velocity of the k-th target, $(\hat{*})_{kl}$ is the estimated values of $(*^o)_k$ in $l-$Monte Carlo run, and L is the number of Monte Carlo runs. L is set to $L = 1000$ unless stated otherwise.

The proposed solution for MTAP in Algorithm 1 uses both BR and RR measurements, denoted as "2-D-DA." We compare its performance with the one from [30] that solely uses BR measurements, expressed as "1-D-DA." The proposed MLE in (34) will be examined against the two-stage WLS method from [33], denoted by "TSWLS." Both the proposed MLE and TSWLS use the solution from 2-D-DA. The RMSEs of targets' positions and velocities are selected as sensing performance metrics. To assess the impact of data association on sensing performance, we initialize with 2-D-DA results and apply MLE iteratively using correctly permuted (i.e., Correct Association) and unpermuted measurements (i.e., Rough Estimation), respectively. Additionally, the CRLB is chosen as a performance benchmark. The convex problem in (27) is addressed using the MATLAB toolbox CVX [34], with the SDPT3 [35] as solver.

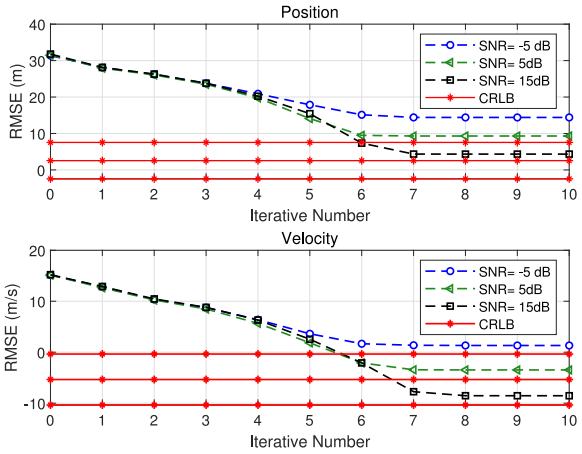

Fig. 2. Evolution of RMSE of position and velocity with $N_t = 6$ $(\mathbf{q}_1, \ldots, \mathbf{q}_6)$, $N_r = 6$ $(\mathbf{p}_1, \ldots, \mathbf{p}_6)$ and $K = 3$ $(\mathbf{s}_1, \mathbf{s}_2, \mathbf{s}_3)$ at SNR = -5 dB, 5 dB, and 15 dB. The red lines with identical markers indicate the bounds, corresponding from top to bottom to SNR = –5 dB, 5 dB, and 15 dB, respectively.

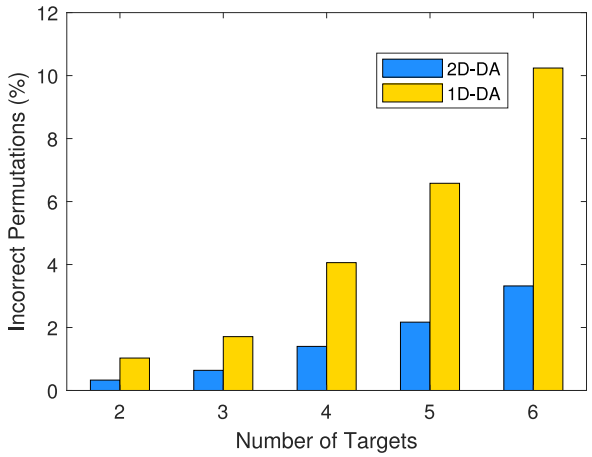

Fig. 4. Incorrect permutations with respect to number of Target K $(\mathbf{s}_1, \ldots, \mathbf{s}_K)$, $N_t = 6$ $(\mathbf{q}_1, \ldots, \mathbf{q}_6)$, $N_r = 6$ $(\mathbf{p}_1, \ldots, \mathbf{p}_6$ and SNR $= -10$ dB. The yellow bars are the results of 1-D-DA from [30] and the blue bars are those of the proposed 2-D-DA. The number of iterations for 2-D-DA is 10.

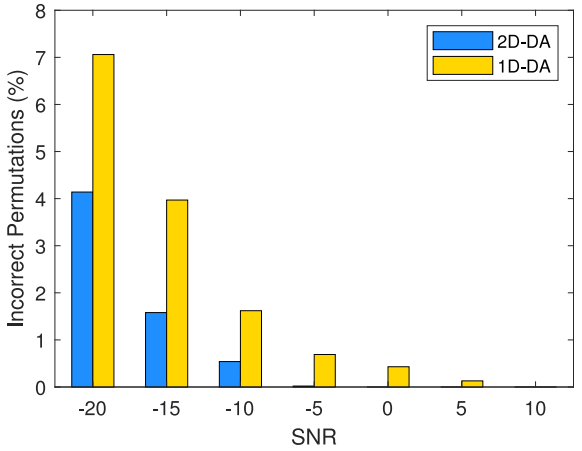

Fig. 3. Incorrect permutations with $N_t = 6$ $(\mathbf{q}_1, \ldots, \mathbf{q}_6)$, $N_r = 6$ $(\mathbf{p}_1, \ldots, \mathbf{p}_6)$ and $K = 3$ $(\mathbf{s}_1, \mathbf{s}_2, \mathbf{s}_3)$. The yellow bars are the results of 1-D-DA from [30] and the blue bars are those of the proposed 2-D-DA. The number of iterations for 2D-DA is 10.

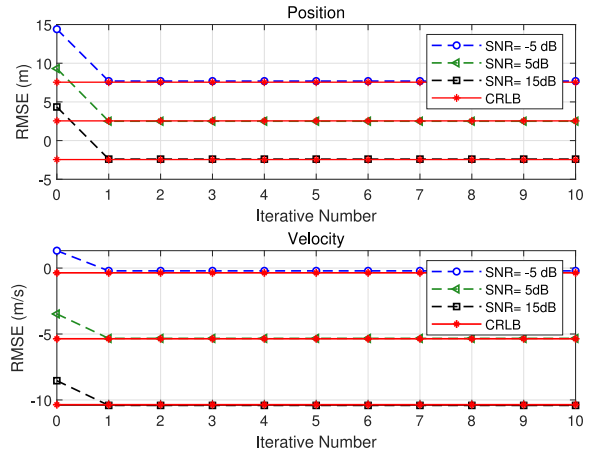

Fig. 5. Evolution of RMSE of position and velocity at SNR = -5 dB, 5 dB, and 15 dB. The initial values are the estimations from 2-D-DA with 8 iterations in Fig. 2. The red lines with identical markers indicate the bounds, corresponding from top to bottom to SNR = –5 dB, 5 dB, and 15 dB, respectively. The number of iterations for 2-D-DA is 10.

B. Data Association

Fig. 2 illustrates the RMSEs of position and velocity with $N_t = 6$ $(\mathbf{q}_1, \ldots, \mathbf{q}_3)$, $N_r = 6$ $(\mathbf{p}_1, \ldots, \mathbf{p}_6)$, and $M = 3$ $(\mathbf{s}_1, \mathbf{s}_2, \mathbf{s}_3)$ with SNR = -5 dB, 5 dB and 15 dB, respectively. The red lines with the markers are the CRLB bounds. As observed, the RMSEs of the position and velocity will converge after a few iterations for the proposed 2D-DA even for SNR $= -5$ dB. Furthermore, the RMSEs in both cases do not reach CRLB bounds, especially for low SNR, due to the relaxed constraints, neglect of noise, and incorrect permutation for low SNR.

Fig. 3 compares the data association accuracy of the proposed 2-D-DA with the 1-D-DA in [30] for $N_t = 6$ $(\mathbf{q}_1, \ldots, \mathbf{q}_6)$, $N_r = 6$ $(\mathbf{p}_1, \ldots, \mathbf{p}_6)$, and $K = 3$ $(\mathbf{s}_1, \mathbf{s}_2, \mathbf{s}_3)$. For the proposed 2-D-DA, 10 repetitions are applied in step 6 of Algorithm 1. As depicted, our proposed 2D-DA significantly outperforms 1D-DA across SNR conditions considered. For instance, the proposed method can achieve nearly 0 incorrect permutations when SNR = -5 dB, whereas the 1D-DA has more incorrect permutations. The performance gap widens at lower SNRs, highlighting the robustness of the proposed 2D-DA method. This is credited to that 2D-DA jointly exploits BR and range RR measurements, which effectively reduce ambiguity in target-measurement association. In contrast, 1D-DA relies solely on BR, offering limited discriminability when targets have similar BR values.

Next, we examine the impact of target numbers on the data association accuracy, as shown in Fig. 4. In this figure, $N_t = 6$, $N_r = 6$, and SNR is -10 dB. Several interesting findings can be observed. First, both 2D-DA and 1D-DA undergo performance degradation as the number of targets increases. The reason is that Additionally, the proposed 2D-DA consistently achieves superior performance than 1D-DA. This is because the BRs and RRs result from the same targets, and both of them can increase the permutation accuracy.

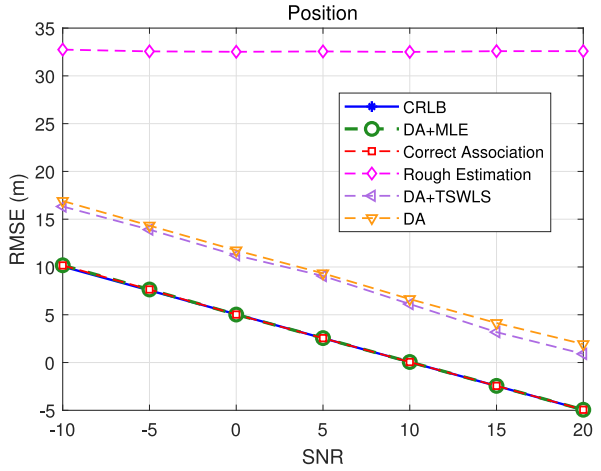

Fig. 6. RMSE of the position against received SNR with $N_t = 3$ $(\mathbf{q}_1, \ldots, \mathbf{q}_6)$, $N_r = 6$ $(\mathbf{p}_1, \ldots, \mathbf{p}_6)$ and $K = 3$ $(\mathbf{s}_1, \mathbf{s}_2, \mathbf{s}_3)$. The red lines show the corresponding bounds. The number of iterations for 2-D-DA and MLE are 10 and 3, respectively.

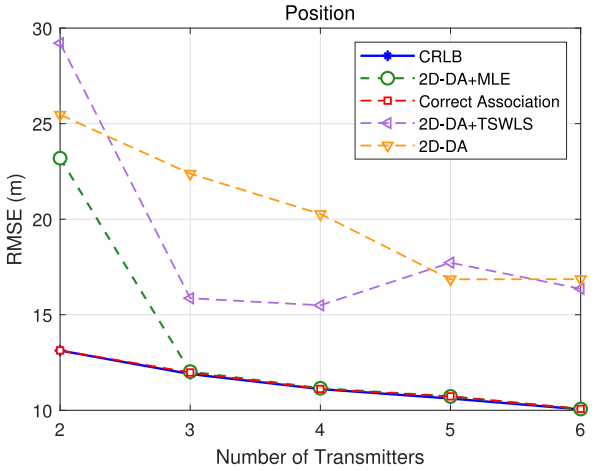

Fig. 8. RMSE of the position with respect to the number of transmitters N_t $(\mathbf{q}_1, \ldots, \mathbf{q}_{N_t})$, $K = 3$ $(\mathbf{s}_1, \ldots, \mathbf{s}_3)$, $N_r = 6$ $(\mathbf{p}_1, \ldots, \mathbf{p}_6)$ and SNR $= -10$ dB. The red lines show the corresponding bounds. The number of iterations for 2-D-DA and MLE are 10 and 3, respectively.

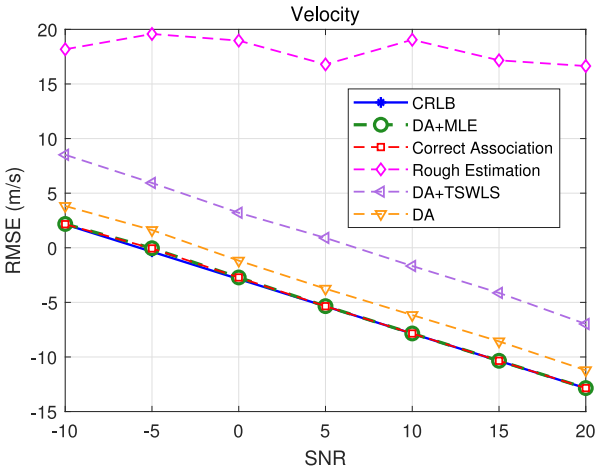

Fig. 7. RMSE of the velocity against received SNR with $N_t = 3$ $(\mathbf{q}_1, \ldots, \mathbf{q}_6)$, $N_r = 6$ $(\mathbf{p}_1, \ldots, \mathbf{p}_6)$ and $K = 3$ $(\mathbf{s}_1, \mathbf{s}_2, \mathbf{s}_3)$. The red lines show the corresponding bounds. The number of iterations for 2-D-DA and MLE are 10 and 3, respectively.

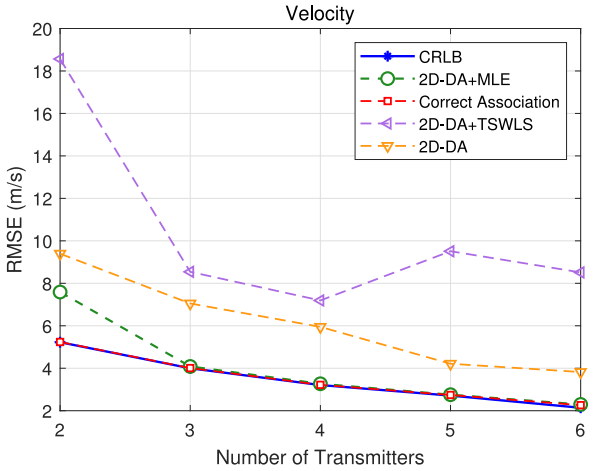

Fig. 9. RMSE of the velocity with respect to the number of transmitters N_t $(\mathbf{q}_1, \ldots, \mathbf{q}_{N_t})$, $K = 3$ $(\mathbf{s}_1, \ldots, \mathbf{s}_3)$, $N_r = 6$ $(\mathbf{p}_1, \ldots, \mathbf{p}_6)$ and SNR $= -10$ dB. The red lines show the corresponding bounds. The number of iterations for 2-D-DA and MLE are 10 and 3, respectively.

C. Position and Velocity Estimation

Fig. 5 demonstrates the RMSEs of position and velocity using the estimations in Fig. 2 as initial values. The red lines show the corresponding bounds. As can be seen, the proposed MLE shows rapid convergence, even within one iteration. Moreover, the results of the proposed MLE approach the CRLB rapidly. This is credited to the preliminary solution from MTAP, which provides an adequate initial value for MLE to achieve satisfactory accuracy.

In the following, we test the target sensing performance of the proposed method at the different SNR conditions, as shown in Figs. 6 and 7. The results with the unpermuted measurements are reasonably poor. It appears that the proposed 2D-DA can provide a preliminary solution for target states, including position and velocity. Based on the 2D-DA solution, the proposed MLE is used to refine target state estimation, with its performance shown by the green lines. The red lines represent the results of the proposed MLE with correctly permuted measurements. Both the red and green lines achieve the CRLB, demonstrating the accuracy of 2D-DA and the effectiveness of the proposed MLE. However, based on the same permuted measurements of 2D-DA, TSWLS shows poor performance with the RMSEs always over 6 m and 5 m/s.

Next, we examine the sensing accuracies of the position and velocity with the number of transmitters in Figs. 8 and 9, respectively. It can be seen that the proposed MLE method with corrected associated measurements can always reach the CRLB even with two transmitters. The preliminary target state estimates by 2D-DA are generally far from the CRLB. However, when the proposed MLE is applied after 2D-DA, the sensing performance can be effectively refined, which can reach CRLB with more than three receivers. The result is attributed to the reduced accuracy of data association by 2-D-DA when the number of transmitters is low. By contrast, the TSWLS can not improve by 2D-DA.

VII. Conclusion

This article investigated sensing problems for multiple moving targets with distributed OTFS radars, aiming to enhance the sensing performance of aerial drones networks. By leveraging the delay and Doppler information from the OTFS channel, we proposed a data association method, i.e., 2-D-DA, to simultaneously address target sensing and data association tasks by formulating an optimization problem. To improve estimation performance, we proposed to employ MLE to refine the preliminary solutions of 2-D-DA as an initialization for the iterative implementation of the MLE. Additionally, we conducted the computational complexities of the proposed data association algorithm and iterative MLE. Simulations demonstrated that the proposed method can achieve the CRLB performance. In summary, by providing accurate estimates of moving target states, the proposed approach enhances sensing performance in aerial drones-based applications.

Appendix

CRLB

The measurement vector $\mathbf{r}$ of BRs and $\dot{\mathbf{r}}$ of RRs are Gaussian distributed and uncorrelated. The logarithm of the probability density function of $\mathbf{r}$ and $\dot{\mathbf{r}}$ given $\boldsymbol{\theta}^o$ is

$$\begin{aligned}\ln p\left(\mathbf{r},\dot{\mathbf{r}}\mid\boldsymbol{\theta}^o\right)= \; & c_0+\left(\mathbf{r}-\mathbf{r}^{\mathrm{T}}\left(\boldsymbol{\theta}^o\right)\right)\mathbf{Q}_{\mathbf{r}}^{-1}\left(\mathbf{r}-\mathbf{r}(\boldsymbol{\theta}^o)\right)\\ & +\left(\dot{\mathbf{r}}-\dot{\mathbf{r}}^{\mathrm{T}}\left(\boldsymbol{\theta}^o\right)\right)\mathbf{Q}_{\dot{\mathbf{r}}}^{-1}\left(\dot{\mathbf{r}}-\dot{\mathbf{r}}(\boldsymbol{\theta}^o)\right)\end{aligned} \tag{41}$$

where c_0 is a constant independent of the unknowns. The Fisher information matrix (FIM) is equal to

$$\begin{aligned}\mathbf{J}\left(\boldsymbol{\theta}^o\right)= & \frac{\partial\mathbf{r}^{\mathrm{T}}\left(\boldsymbol{\theta}^o\right)}{\partial\boldsymbol{\theta}^o}\mathbf{Q}_{\mathbf{r}}^{-1}\frac{\partial\mathbf{r}\left(\boldsymbol{\theta}^o\right)}{\partial\boldsymbol{\theta}^{oT}}\\ & +\frac{\partial\dot{\mathbf{r}}^{\mathrm{T}}\left(\boldsymbol{\theta}^o\right)}{\partial\boldsymbol{\theta}^o}\mathbf{Q}_{\dot{\mathbf{r}}}^{-1}\frac{\partial\dot{\mathbf{r}}\left(\boldsymbol{\theta}^o\right)}{\partial\boldsymbol{\theta}^{oT}}\end{aligned} \tag{42}$$

where the $dK\times N_tN_rK$ gradient matrices are

$$\frac{\partial\mathbf{r}^{\mathrm{T}}\left(\boldsymbol{\theta}^o\right)}{\partial\boldsymbol{\theta}^o}=\left[\frac{\partial r_{11}^{1o}\left(\boldsymbol{\theta}^o\right)}{\partial\boldsymbol{\theta}^o},\frac{\partial r_{12}^{1o}\left(\boldsymbol{\theta}^o\right)}{\partial\boldsymbol{\theta}^o},\ldots,\frac{\partial r_{N_tN_r}^{Ko}\left(\boldsymbol{\theta}^o\right)}{\partial\boldsymbol{\theta}^o}\right] \tag{43a}$$

$$\frac{\partial\dot{\mathbf{r}}^{\mathrm{T}}\left(\boldsymbol{\theta}^o\right)}{\partial\boldsymbol{\theta}^o}=\left[\frac{\partial\dot{r}_{11}^{1o}\left(\boldsymbol{\theta}^o\right)}{\partial\boldsymbol{\theta}^o},\frac{\partial\dot{r}_{12}^{1o}\left(\boldsymbol{\theta}^o\right)}{\partial\boldsymbol{\theta}^o},\ldots,\frac{\partial\dot{r}_{N_tN_r}^{Ko}\left(\boldsymbol{\theta}^o\right)}{\partial\boldsymbol{\theta}^o}\right]. \tag{43b}$$

The elements in (43a) and (43b) can be expressed as

$$\frac{\partial r_{ij}^{ko}\left(\boldsymbol{\theta}^o\right)}{\partial\boldsymbol{\theta}^o}=\left[\mathbf{0},\underbrace{\frac{\partial r_{ij}^{ko}\left(\boldsymbol{\theta}^o\right)}{\partial\mathbf{s}_k^o}^{\mathrm{T}}}_{d(k-1):dk},\mathbf{0}\right]^{\mathrm{T}} \tag{44a}$$

$$\frac{\partial\dot{r}_{ij}^{ko}\left(\boldsymbol{\theta}^o\right)}{\partial\boldsymbol{\theta}^o}=\left[\mathbf{0},\underbrace{\frac{\partial\dot{r}_{ij}^{ko}\left(\boldsymbol{\theta}^o\right)}{\partial\mathbf{s}_k^o}^{\mathrm{T}}}_{d(k-1):dk},\mathbf{0},\underbrace{\frac{\partial\dot{r}_{ij}^{ko}\left(\boldsymbol{\theta}^o\right)}{\partial\dot{\mathbf{s}}_k^o}^{\mathrm{T}}}_{d(K+k-1):d(K+k)},\mathbf{0}\right]^{\mathrm{T}} \tag{44b}$$

where

$$\frac{\partial r_{ij}^{ko}\left(\boldsymbol{\theta}^o\right)}{\partial\mathbf{s}_k^o}^{\mathrm{T}}=\boldsymbol{\rho}_{\mathbf{s}_k^o,\mathbf{q}_i}^{\mathrm{T}}+\boldsymbol{\rho}_{\mathbf{s}_k^o,\mathbf{p}_j}^{\mathrm{T}} \tag{45a}$$

$$\frac{\partial\dot{r}_{ij}^{ko}\left(\boldsymbol{\theta}^o\right)}{\partial\mathbf{s}_k^o}^{\mathrm{T}}=\boldsymbol{\xi}_{\mathbf{s}_k^o,\mathbf{q}_i}^{\mathrm{T}}+\boldsymbol{\xi}_{\mathbf{s}_k^o,\mathbf{p}_j}^{\mathrm{T}} \tag{45b}$$

$$\frac{\partial\dot{r}_{ij}^{ko}\left(\boldsymbol{\theta}^o\right)}{\partial\dot{\mathbf{s}}_k^o}^{\mathrm{T}}=\frac{\partial r_{ij}^{ko}\left(\boldsymbol{\theta}^o\right)}{\partial\mathbf{s}_k^o}^{\mathrm{T}} \tag{45c}$$

where $\boldsymbol{\xi}_{\mathbf{s}_k^o,\mathbf{q}_i}$ and $\boldsymbol{\xi}_{\mathbf{s}_k^o,\mathbf{p}_j}$ are defined in (36a) and (36b). Under the Gaussian measurement noise model, the CRLB of $\boldsymbol{\theta}^o$ is given by

$$\mathrm{CRLB}\left(\boldsymbol{\theta}^o\right)=\mathbf{J}\left(\boldsymbol{\theta}^o\right)^{-1}. \tag{46}$$

The CRLB provides the best achievable accuracy for target position and velocity estimations.

References

[1] H. Shakhatreh et al., "Unmanned aerial vehicles (UAVs): A survey on civil applications and key research challenges," *IEEE Access*, vol. 7, pp. 48572–48634, 2019.

[2] J. Wu, W. Yuan, and L. Bai, "On the interplay between sensing and communications for UAV trajectory design," *IEEE Internet Things J.*, vol. 10, no. 23, pp. 20383–20395, Dec. 2023.

[3] Y. Zeng, R. Zhang, and T. J. Lim, "Wireless communications with unmanned aerial vehicles: Opportunities and challenges," *IEEE Commun. Mag.*, vol. 54, no. 5, pp. 36–42, May 2016.

[4] Q. Wu, Y. Zeng, and R. Zhang, "Joint trajectory and communication design for multi-UAV enabled wireless networks," *IEEE Trans. Wireless Commun.*, vol. 17, no. 3, pp. 2109–2121, Mar. 2018.

[5] Y. Gong, X. Li, F. Meng, L. Liu, M. Guizani, and Z. Xu, "Toward green RF chain design for integrated sensing and communications: Technologies and future directions," *IEEE Commun. Mag.*, vol. 62, no. 9, pp. 36–42, Sep. 2024.

[6] D. Zhang et al., "Integrated sensing and communications over the years: An evolution perspective," 2025, *arXiv:2504.06830*.

[7] F. Liu et al., "Seventy years of radar and communications: The road from separation to integration," *IEEE Signal Process. Mag.*, vol. 40, no. 5, pp. 106–121, Jul. 2023.

[8] C. Liu et al., "Learning-based predictive beamforming for integrated sensing and communication in vehicular networks," *IEEE J. Sel. Areas Commun.*, vol. 40, no. 8, pp. 2317–2334, Aug. 2022.

[9] S. Lu et al., "Integrated sensing and communications: Recent advances and ten open challenges," *IEEE Internet Things J.*, vol. 11, no. 11, pp. 19094–19120, Jun. 2024.

[10] Y. Xiong, F. Liu, Y. Cui, W. Yuan, T. X. Han, and G. Caire, "On the fundamental tradeoff of integrated sensing and communications under Gaussian channels," *IEEE Trans. Inf. Theory*, vol. 69, no. 9, pp. 5723–5751, Sep. 2023.

[11] Y. Cui, W. Yuan, Z. Zhang, J. Mu, and X. Li, "On the physical layer of digital twin: An integrated sensing and communications perspective," *IEEE J. Sel. Areas Commun.*, vol. 41, no. 11, pp. 3474–3490, Nov. 2023.

[12] D. Van Welden, H. Steendam, and M. Moeneclaey, "Time delay estimation for KSP-OFDM systems in multipath fading channels," in *Proc. IEEE 20th Int. Symp. Pers., Indoor Mobile Radio Commun.*, 2009, pp. 3064–3068.

[13] M. D. Larsen, G. Seco-Granados, and A. L. Swindlehurst, "Pilot optimization for time-delay and channel estimation in OFDM systems," in *Proc. IEEE Int. Conf. Acoust., Speech Signal Process. (ICASSP)*, 2011, pp. 3564–3567.

[14] M. C. Vanderveen, C. B. Papadias, and A. Paulraj, "Joint angle and delay estimation (JADE) for multipath signals arriving at an antenna array," *IEEE Commun. Lett.*, vol. 1, no. 1, pp. 12–14, Jan. 1997.

[15] Y. Mostofi and D. C. Cox, "ICI mitigation for pilot-aided OFDM mobile systems," *IEEE Trans. Wireless Commun.*, vol. 4, no. 2, pp. 765–774, Mar. 2005.

[16] C. Sturm and W. Wiesbeck, "Waveform design and signal processing aspects for fusion of wireless communications and radar sensing," *Proc. IEEE*, vol. 99, no. 7, pp. 1236–1259, Jul. 2011.

[17] J.-F. Gu, J. Moghaddasi, and K. Wu, "Delay and Doppler shift estimation for OFDM-based radar-radio (RadCom) system," in *Proc. IEEE Int. Wireless Symp. (IWS)*, 2015, pp. 1–4.

[18] P. Raviteja, K. T. Phan, Y. Hong, and E. Viterbo, "Interference cancellation and iterative detection for orthogonal time frequency space modulation," *IEEE Trans. Wireless Commun.*, vol. 17, no. 10, pp. 6501–6515, Oct. 2018.
[19] W. Yuan et al., "New delay Doppler communication paradigm in 6G era: A survey of orthogonal time frequency space (OTFS)," *China Commun.*, vol. 20, no. 6, pp. 1–25, Jun. 2023.
[20] W. Yuan, S. Li, Z. Wei, J. Yuan, and D. W. K. Ng, "Data-aided channel estimation for OTFS systems with a superimposed pilot and data transmission scheme," *IEEE Wireless Commun. Letters*, vol. 10, no. 9, pp. 1954–1958, Sep. 2021.
[21] L. Zhao, W.-J. Gao, and W. Guo, "Sparse Bayesian learning of delay-Doppler channel for OTFS system," *IEEE Commun. Lett.*, vol. 24, no. 12, pp. 2766–2769, Dec. 2020.
[22] W. Shen, L. Dai, J. An, P. Fan, and R. W. Heath, "Channel estimation for orthogonal time frequency space (OTFS) massive MIMO," *IEEE Trans. Signal Process.*, vol. 67, no. 16, pp. 4204–4217, Aug. 2019.
[23] W. Yuan, L. Zhou, S. K. Dehkordi, S. Li, P. Fan, G. Caire, and H. V. Poor, "From OTFS to DD-ISAC: Integrating sensing and communications in the delay Doppler domain," *IEEE Wireless Commun.*, vol. 31, no. 6, pp. 152–160, Dec. 2024.
[24] B. Li and W. Yuan, "OTFS communications-assisted environment sensing," in *Proc. IEEE 3rd Int. Symp. Joint Commun. Sens. (JCS)*, 2023, pp. 1–6.
[25] Z. Gong, F. Jiang, C. Li, and X. Shen, "Simultaneous localization and communications with massive MIMO-OTFS," *IEEE J. Sel. Areas Commun.*, vol. 41, no. 12, pp. 3908–3924, Dec. 2023.
[26] K. Wu, J. A. Zhang, X. Huang, and Y. J. Guo, "OTFS-based joint communication and sensing for future Industrial IoT," *IEEE Internet Things J.*, vol. 10, no. 3, pp. 1973–1989, Feb. 2023.
[27] W. Yi, T. Zhou, Y. Ai, and R. S. Blum, "Suboptimal low complexity joint multi-target detection and localization for non-coherent MIMO radar with widely separated antennas," *IEEE Trans. Signal Process.*, vol. 68, pp. 901–916, 2020.
[28] L. Rui and K. Ho, "Elliptic localization: Performance study and optimum receiver placement," *IEEE Trans. Signal Process.*, vol. 62, no. 18, pp. 4673–4688, Sep. 2014.
[29] S. Deb, M. Yeddanapudi, K. Pattipati, and Y. Bar-Shalom, "A generalized SD assignment algorithm for multisensor-multitarget state estimation," *IEEE Trans. Aerosp. Electron. Syst.*, vol. 33, no. 2, pp. 523–538, Apr. 1997.
[30] S. A. R. Kazemi, R. Amiri, and F. Behnia, "Data association for multi-target elliptic localization in distributed MIMO radars," *IEEE Commun. Lett.*, vol. 25, no. 9, pp. 2904–2907, Sep. 2021.
[31] K. Zhang et al., "Radar sensing via OTFS signaling: A delay Doppler signal processing perspective," in *Proc. IEEE Int. Conf. Commun.*, 2023, pp. 6429–6434.
[32] T. S. Rappaport, "Wireless communications–principles and practice, (the book end)," *Microw. J.*, vol. 45, no. 12, pp. 128–129, 2002.
[33] H. Song, G. Wen, L. Zhu, and D. Li, "A novel TSWLS method for moving target localization in distributed MIMO radar systems," *IEEE Commun. Lett.*, vol. 23, no. 12, pp. 2210–2214, Dec. 2019.
[34] M. Grant and S. Boyd. "CVX: MATLAB software for disciplined convex programming, version 2.1." Accessed: Apr. 1, 2025. [Online]. Available: https://github.com/cvxr/CVX
[35] K.-C. Toh, M. J. Todd, and R. H. Tütüncü, "SDPT3—A MATLAB software package for semidefinite programming, version 1.3," *Optim. Methods Softw.*, vol. 11, nos. 1–4, pp. 545–581, 1999.

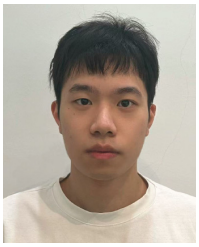

Buyi Li received the B.Eng. degree in electrical and electronic engineering from the Southern University of Science and Technology, Shenzhen, China, in 2022, where he is currently pursuing the master's degree with the School of System Design and Intelligent Manufacturing.

His research focuses on the area of sensing problems based on Orthogonal Time Frequency Space.

Mr. Li was a recipient of the Best Paper Award from IEEE GLOBECOM 2024.

Dongxuan He received the B.S. degree in automation and the Ph.D. degree in information and communication systems from Beijing Institute of Technology (BIT), Beijing, China, in 2013 and 2019, respectively.

From 2017 to 2018, he was a visiting student with Singapore University of Technology and Design, Singapore. From 2019 to 2022, he was a Postdoctoral Researcher with the Department of Electronic Engineering, Tsinghua University, Beijing. He is currently an Assistant Professor with the School of Information and Electronics, BIT. His current interests include Integrated sensing and communication (ISAC), Terahertz communication, and AI empowered wireless communications.

Dr. He was a recipient of the Best Paper Award from 2024 IEEE ICSIDP, 2025 IEEE IWCMC. He was also an exemplary reviewer of IEEE WIRELESS COMMUNICATIONS LETTERS. He is currently serving as a Guest Editor for the IEEE Open Journal of the Communications Society, *Electronics*, and *Space: Science & Technology*.

Qin Tao received the B.S. degree from the Electronic Information School, Wuhan University, Wuhan, China, in 2017, and the Ph.D. degree in communication and information systems from Zhejiang University, Hangzhou, China, in 2022.

She is currently an Associate Professor with the School of Information Science and Technology, Hangzhou Normal University, Hangzhou. Her research interests include backscatter communication, intelligent reflecting surface, symbiotic radio and orthogonal time frequency space modulation.

Dr. Tao and her co-authors have been awarded the Best Paper Award at the ICCC 2018, WCSP 2020 and WCSP 2023.